cancers

MDPI

Article

Association Between Stromal Fibrosis and FDG PET/CT-Derived SUV Parameters in Pancreatic Ductal Adenocarcinoma: An Exploratory Study

Tae Joo Jeon [1,*], Se Joon Lee [2] and Beom Jin Lim [3]

[1] Department of Nuclear Medicine, Gangnam Severance Hospital, Yonsei University College of Medicine, 211 Eonju-ro, Gangnam-gu, Seoul 06273, Republic of Korea
[2] Department of Internal Medicine, Yongin Severance Hospital, Yonsei University College of Medicine, 1151 Jung-dong, Giheung-gu, Yongin 16995, Republic of Korea; leesj@yuhs.ac
[3] Department of Pathology, Yonsei University College of Medicine, 134 Sinchon-dong, Seodaemun-gu, Seoul 03722, Republic of Korea; bjlim@yuhs.ac
* Correspondence: tjeonnm@yuhs.ac; Tel.: +82-2-2019-3740; Fax: +82-2-2019-4856

Simple Summary

Pancreatic cancer contains large amounts of dense, scar-like fibrous tissue (fibrosis) that influences tumor growth and treatment resistance, but this tissue is difficult to assess before surgery. Positron emission tomography (PET) with fluorodeoxyglucose (FDG), a radioactive glucose analogue, shows how actively tumors take up glucose. We examined whether FDG uptake reflects the amount of fibrosis in 21 surgically removed pancreatic cancers. Tumors with more fibrosis tended to show lower FDG uptake, and this relationship was moderate in strength and similar for the three standard uptake measures. However, FDG uptake explained less than half of the differences in fibrosis between tumors, so it cannot replace tissue examination. These preliminary findings support validation in larger groups of patients and the use of imaging agents that target the fibrous tissue directly.

Abstract

Background/Objectives: Dense stromal fibrosis is a hallmark of pancreatic ductal adenocarcinoma (PDAC) but cannot be assessed noninvasively before surgery. We explored whether ^{18}F-fluorodeoxyglucose (FDG) positron emission tomography/computed tomography (PET/CT) uptake reflects the degree of fibrosis in resected PDAC. **Methods:** Twenty-one patients with surgically resected, histologically confirmed PDAC and preoperative FDG PET/CT were retrospectively analyzed. Tumors were segmented using a 50% maximum standardized uptake value (SUVmax) threshold, or a gradient-based method when thresholding failed, to obtain SUVmax, peak SUV (SUVpeak; 1 cm^3 sphere), mean SUV (SUVmean), and metabolic tumor volume. Fibrosis was quantified as the collagen proportionate area on Masson trichrome-stained sections. Associations were assessed using Spearman and Pearson correlation coefficients with 95% confidence intervals (CIs). **Results:** Fibrosis ranged from 0.5% to 68.5% (median, 31.7%), and intraobserver agreement was excellent (intraclass correlation coefficient, 0.987). All absolute SUV parameters were inversely associated with fibrosis (SUVpeak, $\rho = -0.66$ [95% CI, -0.86 to -0.28], $p = 0.001$; SUVmax, $\rho = -0.65$, $p = 0.001$; SUVmean, $\rho = -0.54$, $p = 0.011$). The associations persisted after adjustment for metabolic tumor volume and scanner type but were weaker in linear (Pearson) analyses. The three SUV parameters performed similarly, and SUV ratios were not associated with fibrosis. **Conclusions:** In this exploratory study, higher FDG uptake was associated with less stromal fibrosis in PDAC, although the strength of the association depended on the analytic method and was influenced by a single high-uptake tumor. These

Check for updates

Academic Editor: Michael Bouvet

Received: 4 November 2026
Revised: 14 November 2026
Accepted: 16 November 2026
Published: 18 November 2026

Copyright: © 2026 by the authors. Licensee MDPI, Basel, Switzerland. This article is an open access article distributed under the terms and conditions of the Creative Commons Attribution (CC BY) license.

preliminary findings suggest that FDG PET/CT may provide indirect information on stromal characteristics but cannot replace histological assessment; validation in larger cohorts is required.

Keywords: pancreatic ductal adenocarcinoma; fibrosis; tumor microenvironment; FDG PET/CT; standardized uptake value; SUVpeak; exploratory study

1. Introduction

Pancreatic ductal adenocarcinoma (PDAC) remains one of the most lethal malignancies, with a 5-year relative survival rate of approximately 13% in the United States [1,2]. Because most patients present with advanced disease, earlier diagnosis and better preoperative characterization of tumor biology are urgently needed [1,2]. A defining histological feature of PDAC is its dense desmoplastic stroma, which may constitute the majority of the tumor mass and consists of cancer-associated fibroblasts (CAFs), extracellular matrix, and immune and vascular components [2,3]. Stromal fibrosis has been implicated in tumor progression, impaired drug delivery, and treatment resistance, and the amount and pattern of stroma have been associated with prognosis [3–8]. Preoperative information on stromal burden could therefore help characterize tumor biology. However, obtaining diagnostic tissue from the pancreas is technically demanding, and even when it is obtained, small biopsy specimens cannot represent the stromal composition of the entire tumor.

^{18}F-fluorodeoxyglucose (FDG) positron emission tomography/computed tomography (PET/CT) is widely used for the staging of PDAC, and quantitative parameters such as the maximum standardized uptake value (SUVmax), metabolic tumor volume (MTV), and indices of intratumoral metabolic heterogeneity have been associated with tumor differentiation, treatment response, and survival [9–14]. Because FDG accumulates mainly in metabolically active tumor cells, a fibrotic, hypocellular, and hypovascular stroma might be expected to lower FDG uptake per unit volume, and CAFs can also reprogram the glucose metabolism of adjacent tumor cells [15]. Nevertheless, the relationship between FDG uptake and the degree of stromal fibrosis in human PDAC has not been well characterized.

In this exploratory study, we quantified stromal fibrosis in surgically resected PDAC specimens and examined its association with FDG PET/CT-derived SUV parameters, including peak SUV (SUVpeak) measured according to the standard 1 cm^3 definition [16], and with simple SUV ratios proposed as surrogates of metabolic heterogeneity. Our aims were to estimate the direction and magnitude of these associations and to provide data for the design of adequately powered validation studies. Whether FDG PET/CT can replace tissue assessment, and its clinical utility, were not evaluated.

2. Materials and Methods

2.1. Patients

This retrospective study included patients who underwent surgical resection for PDAC and preoperative FDG PET/CT at Gangnam Severance Hospital between November 2009 and December 2016. The study period was limited to this interval because the dedicated pancreatobiliary team, including the endoscopist and the pancreatic surgeon who collected specimens under the study protocol, relocated to other institutions thereafter. The study was originally designed to accrue a larger cohort and to examine the relationship between fibrosis and a wider range of PET texture features; however, case accrual was slow, and after this relocation the study could not be continued. The available cases were therefore analyzed in the present exploratory study. The inclusion criteria were (1) histologically

confirmed PDAC after surgical resection, (2) FDG PET/CT performed before surgery without intervening treatment, and (3) availability of tumor tissue adequate for fibrosis quantification. After the exclusion of patients without adequate specimens or staining, 23 patients were identified. The exact number of patients screened and excluded at this initial step could not be reliably reconstructed from the archived research records. Of these, two were excluded after pathological re-review revealed a neuroendocrine tumor and a mucinous neoplasm, respectively. Thus, 21 patients were included in the analysis. No patient received neoadjuvant therapy, as confirmed by the absence of ypTNM staging and treatment-effect grading in the pathology reports. Pathological stage was assigned according to the 8th edition of the American Joint Committee on Cancer (AJCC) staging manual [17]. The study was approved by the Institutional Review Board of Gangnam Severance Hospital (3-2015-0436), which waived the requirement for informed consent.

2.2. FDG PET/CT Acquisition

FDG PET/CT was performed using a Biograph TruePoint 40 or a Biograph mCT scanner (Siemens Healthcare, Malvern, PA, USA). Patients fasted for at least 6 h, and according to the institutional protocol, PET/CT was not performed if the blood glucose level was 150 mg/dL (8.3 mmol/L) or higher. FDG (5.18 MBq/kg) was injected intravenously, and imaging began 60 min later. Low-dose CT (120 kVp, 180 mAs) was acquired for attenuation correction and anatomical localization. PET images were reconstructed using ordered-subset expectation maximization (OSEM) with two iterations and 21 subsets.

2.3. PET Image Analysis

All images were reanalyzed for this revised study using MIM software (version 7.3.7; MIM Software Inc., Cleveland, OH, USA) by a nuclear medicine physician (T.J.J.) blinded to the fibrosis measurements. The primary tumor was segmented with a 50% isocontour of SUVmax, in accordance with the European Association of Nuclear Medicine guideline [18]. When the threshold contour failed to delineate the lesion because of low tumor-to-background contrast, typically by extending into adjacent physiological uptake, the gradient-based PET Edge tool was used instead; gradient-based segmentation has been shown to be more accurate than fixed thresholds in low-contrast lesions [19]. Contours were manually edited when necessary to exclude contiguous physiological uptake in the bowel or kidney. SUVmax, SUVpeak, and mean SUV (SUVmean) were normalized to body weight. SUVpeak was defined as the highest mean SUV within a 1 cm^3 sphere within the volume of interest [16]. MTV was defined as the volume of the segmented tumor. The maximum tumor diameter was measured on the CT component.

The SUVmax/SUVmean and SUVmax/SUVpeak ratios were calculated as simple indices of the shape of the intratumoral uptake distribution, based on the hypothesis that fibrotic stroma interspersed among tumor cells would broaden the distribution of voxel uptake values relative to the maximum. We acknowledge that these ratios are crude summary measures and do not directly quantify spatial heterogeneity.

2.4. Histological Assessment of Fibrosis

Formalin-fixed, paraffin-embedded tumor sections were stained with hematoxylin and eosin and Masson trichrome. For each patient, one to three representative tumor sections were selected by a pathologist (B.J.L.) blinded to the PET/CT findings, and 5–10 non-overlapping fields covering the tumor were photographed using a BX45 microscope (Olympus, Tokyo, Japan) at ×200 magnification (20× objective lens). Fibrosis was quantified using ImageJ (version 1.8.0; National Institutes of Health, Bethesda, MD, USA) [20] as the collagen proportionate area. Blue-stained extracellular matrix was isolated by color

thresholding (hue, 121–179; saturation, 20–255; brightness, 10–255) and divided by the total tissue area of each field, excluding background and luminal spaces. The patient-level value was the mean percentage across all fields. Picrosirius red staining was used only for qualitative confirmation of collagen distribution and was not quantified. To assess intraobserver reproducibility, all cases were re-measured by the same observer after an interval of 4 weeks, blinded to the initial measurements.

2.5. Statistical Analysis

Continuous variables are presented as medians with interquartile ranges (IQRs), and categorical variables as numbers with percentages. Normality was assessed with the Shapiro–Wilk test. SUVpeak and SUVmean were designated as the primary parameters at the outset of the present reanalysis, before the re-measurement of all PET images; because this designation was made after the initial analysis of the original data set, it does not constitute prespecification in the strict sense, and the study as a whole should be regarded as exploratory; SUVmax and the two SUV ratios were regarded as exploratory. Because SUV distributions were markedly right-skewed, associations with fibrosis were evaluated primarily with Spearman rank correlation coefficients (ρ), with 95% confidence intervals (CIs) calculated using the Bonett–Wright method; Pearson coefficients (r) with Fisher z-based CIs are also reported. Correlation strength was interpreted according to Schober et al. [21]. p-values for the two primary parameters were adjusted using the Holm method. Dependent correlations sharing fibrosis as a common variable were compared using Williams' test [22]. Partial correlations (Pearson and rank-based) were calculated to adjust for log-transformed MTV, pathological tumor size, and scanner type. Sensitivity analyses included (1) the use of the repeated fibrosis measurement, (2) exclusion of influential observations (Cook's distance $> 4/n$), and (3) restriction to tumors segmented with the 50% threshold alone. Intraobserver agreement was assessed using the intraclass correlation coefficient (ICC; two-way random effects, absolute agreement, single measurement) [23] and Bland–Altman analysis [24]. The sample size required for a validation study was estimated using Fisher's z transformation for Pearson correlation and the Bonett–Wright approximation for Spearman correlation (two-sided $\alpha = 0.05$, power = 80%). A two-sided $p < 0.05$ was considered statistically significant. Analyses were performed using Python (version 3.13; Python Software Foundation, Wilmington, DE, USA) with SciPy (version 1.18; https://scipy.org).

2.6. Use of Generative Artificial Intelligence

Claude (Anthropic; model claude-opus-5-5) was used to assist with writing statistical analysis code, preparing figures, and drafting and editing the manuscript text. All analyses and text were reviewed and verified by the authors, who take full responsibility for the content.

3. Results

3.1. Patient Characteristics

The characteristics of the 21 patients are summarized in Table 1. The median age was 65 years (IQR, 56–72), and 13 patients (62%) were men. Tumors were located in the pancreatic head in 12 patients (57%), and the median pathological tumor size was 3.1 cm (IQR, 2.3–3.8). Most tumors were moderately differentiated (16 patients, 76%). The median interval between PET/CT and surgery was 8 days (range, 1–58).

Table 1. Patient and tumor characteristics ($n = 21$).

Characteristic	Value
Age (yr)	65 (56–72)
Sex	
Male	13 (62)
Female	8 (38)
Tumor location	
Head	12 (57)
Body	1 (5)
Tail	7 (33)
Diffuse	1 (5)
Operation	
Pylorus-preserving pancreaticoduodenectomy	10 (48)
Pancreaticoduodenectomy	1 (5)
Distal pancreatectomy	8 (38)
Total pancreatectomy	2 (10)
Pathological tumor size (cm)	3.1 (2.3–3.8)
pT category (AJCC 8th)	
T1	2 (10)
T2	15 (71)
T3	4 (19)
pN category	
N0	10 (48)
N1	6 (29)
N2	5 (24)
Stage (AJCC 8th)	
IA	2 (10)
IB	7 (33)
IIA	1 (5)
IIB	6 (29)
III	5 (24)
Histological grade	
Well differentiated	4 (19)
Moderately differentiated	16 (76)
Poorly differentiated	1 (5)
Lymphovascular invasion	10 (48)
Perineural invasion	15 (71)
Resection margin	
R0	18 (86)
R1	3 (14)
CA19-9 (U/mL)	85.0 (15.1–460.2)
CA19-9 > 37 U/mL	12 (57)
Neoadjuvant therapy	0 (0)
PET/CT-to-surgery interval (day)	8 (7–14)
PET/CT scanner	
Biograph TruePoint 40	12 (57)
Biograph mCT	9 (43)
Segmentation method	
50% SUVmax threshold	14 (67)
PET Edge (gradient-based)	7 (33)
Tumor diameter on PET/CT (cm)	2.6 (2.1–3.2)
SUVmax	5.23 (4.20–6.77)
SUVpeak	4.51 (3.70–5.71)
SUVmean	3.53 (2.87–4.31)

Table 1. *Cont.*

Characteristic	Value
MTV (mL)	5.82 (2.60–10.96)
SUVmax/SUVmean	1.54 (1.29–1.56)
SUVmax/SUVpeak	1.15 (1.11–1.21)
Fibrosis (%)	31.7 (12.7–41.1)

Values are presented as median (interquartile range) or number (%). AJCC, American Joint Committee on Cancer; CA19-9, carbohydrate antigen 19-9; PET/CT, positron emission tomography/computed tomography; SUV, standardized uptake value; SUVmax, maximum SUV; SUVpeak, peak SUV (1 cm^3 sphere); SUVmean, mean SUV; MTV, metabolic tumor volume.

3.2. PET Parameters and Fibrosis

The 50% threshold delineated the tumor in 14 patients (67%); in the remaining 7 (33%), it failed because of low tumor-to-background contrast, and PET Edge segmentation was used. The median SUVmax, SUVpeak, and SUVmean were 5.23, 4.51, and 3.53, respectively, and the median MTV was 5.8 mL (Table 1). The three SUV parameters were highly intercorrelated (Pearson $r \geq 0.984$). The degree of fibrosis varied widely, from 0.5% to 68.5% (median, 31.7%; IQR, 12.7–41.1). Fibrosis was not significantly correlated with pathological tumor size ($\rho = -0.33$, $p = 0.144$) or CA19-9 level ($\rho = -0.29$, $p = 0.207$). Intraobserver agreement for fibrosis quantification was excellent (ICC, 0.987; 95% CI, 0.968–0.995), with a mean difference of 0.3 percentage points (95% limits of agreement, −5.5 to 6.1).

3.3. Association Between FDG Uptake and Fibrosis

All three absolute SUV parameters were inversely associated with fibrosis (Table 2, Figure 1). SUVpeak showed a moderate-to-strong inverse association ($\rho = -0.66$; 95% CI, −0.86 to −0.28; $p = 0.001$), and SUVmean showed a moderate inverse association ($\rho = -0.54$; 95% CI, −0.80 to −0.11; $p = 0.011$); both remained significant after Holm adjustment ($p = 0.002$ and $p = 0.011$, respectively). SUVmax showed an association similar to that of SUVpeak ($\rho = -0.65$; $p = 0.001$). The corresponding Pearson coefficients were smaller ($r = -0.44$ to -0.47; $p = 0.032$–0.047), and the Holm-adjusted Pearson p-values for the primary parameters were 0.076. The strength of association did not differ among SUVpeak, SUVmean, and SUVmax (Williams' test, all $p \geq 0.26$). The associations persisted after adjustment for log-transformed MTV (partial $r = -0.46$ to -0.49; $p = 0.027$–0.042) or scanner type (partial $r = -0.44$ to -0.47; $p = 0.037$–0.053). After adjustment for pathological tumor size, the Pearson partial correlations were attenuated ($r = -0.38$ to -0.42; $p = 0.068$–0.099), whereas the rank-based partial correlations remained significant ($\rho = -0.50$ to -0.62; $p = 0.004$–0.024). Neither SUV ratio was associated with fibrosis (SUVmax/SUVmean, $\rho = -0.26$; SUVmax/SUVpeak, $\rho = -0.22$) (Figure 2).

Table 2. Correlations between PET parameters and fibrosis ($n = 21$).

Parameter	Spearman ρ (95% CI)	p	Pearson r (95% CI)	p	Partial r * (95% CI)	p
SUVpeak †	−0.66 (−0.86 to −0.28)	0.001	−0.44 (−0.73 to −0.01)	0.047	−0.46 (−0.76 to −0.01)	0.048
SUVmean †	−0.54 (−0.80 to −0.11)	0.011	−0.46 (−0.74 to −0.03)	0.038	−0.49 (−0.77 to −0.05)	0.033
SUVmax	−0.65 (−0.86 to −0.26)	0.001	−0.47 (−0.75 to −0.05)	0.032	−0.49 (−0.77 to −0.04)	0.034
SUVmax/SUVmean	−0.26 (−0.63 to 0.20)	0.251	−0.36 (−0.69 to 0.08)	0.108	−0.34 (−0.69 to 0.14)	0.158
SUVmax/SUVpeak	−0.22 (−0.60 to 0.24)	0.333	−0.22 (−0.59 to 0.24)	0.342	−0.18 (−0.59 to 0.30)	0.452

CI, confidence interval; SUV, standardized uptake value; SUVpeak, peak SUV (1 cm^3 sphere); SUVmean, mean SUV; SUVmax, maximum SUV. * Pearson partial correlation adjusted for log-transformed metabolic tumor volume and scanner type. † Primary parameters; Holm-adjusted p-values were 0.002 (SUVpeak) and 0.011 (SUVmean) for the Spearman coefficients and 0.076 for both Pearson coefficients.

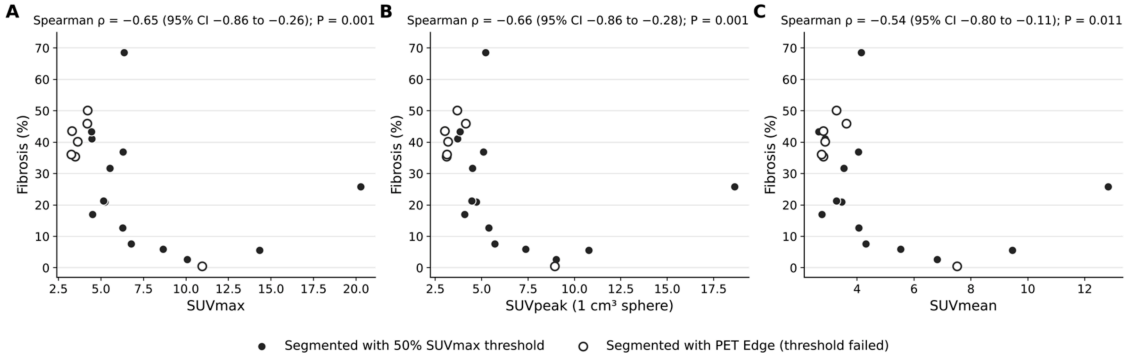


Figure 1. Scatter plots of fibrosis against (**A**) the maximum standardized uptake value (SUVmax), (**B**) the peak SUV (SUVpeak; 1 cm^3 sphere), and (**C**) the mean SUV (SUVmean) in 21 patients with pancreatic ductal adenocarcinoma. Filled circles indicate tumors segmented with a 50% SUVmax threshold, and open circles indicate tumors segmented with the gradient-based PET Edge method because thresholding failed. Spearman correlation coefficients (ρ) with 95% confidence intervals (CIs) are shown.

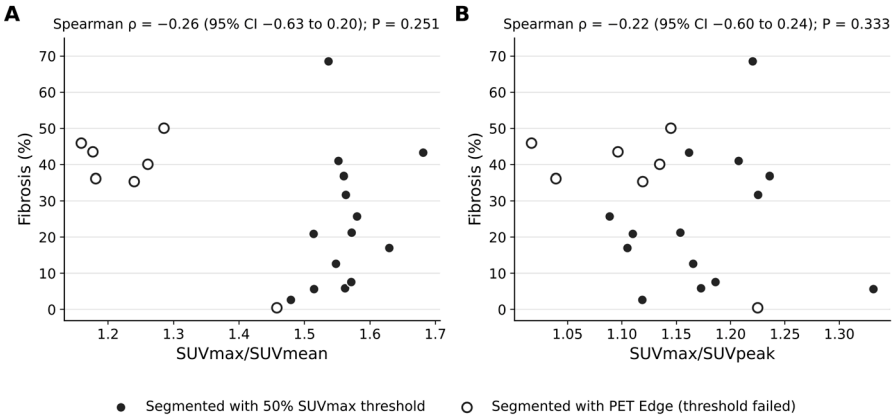


Figure 2. Scatter plots of fibrosis against (**A**) the SUVmax/SUVmean ratio and (**B**) the SUVmax/SUVpeak ratio. Symbols are as in Figure 1. Spearman correlation coefficients (ρ) with 95% confidence intervals (CIs) are shown.

3.4. Sensitivity Analyses

The results of the sensitivity analyses are shown in Table 3. Using the repeated fibrosis measurement yielded nearly identical estimates (agreement between the two measurements is shown in Figure 3). One patient with markedly high FDG uptake (SUVmax, 20.3) and intermediate fibrosis (25.8%) was a highly influential observation (Cook's distance, 7.1). Excluding this patient strengthened the Pearson correlations ($r = -0.63$ to -0.70; $p \leq 0.003$), so that they became similar to the rank-based coefficients ($\rho = -0.57$ to -0.69). When the analysis was restricted to the 14 tumors segmented with the 50% threshold alone, the Spearman coefficients were of similar magnitude (SUVpeak, $\rho = -0.60$, $p = 0.023$; SUVmean, $\rho = -0.53$, $p = 0.054$). In this subset, however, the Pearson coefficients were smaller and not significant ($r = -0.27$ to -0.30; $p = 0.29$–0.35). SUV values remained markedly right-skewed within the subset (Shapiro–Wilk $p \leq 0.001$), and the high-uptake tumor described above was included and was again highly influential (Cook's distance, 5.2); after its exclusion ($n = 13$), the Pearson and Spearman coefficients were −0.51 to −0.57 and −0.66 to −0.74, respectively. To validate a correlation of 0.45 with 80% power, approximately 37 patients would be required for a Pearson correlation and approximately 40 patients for a Spearman correlation. These estimates assume a simple bivariate association and do not account for

potential confounders, such as tumor size and partial-volume effects; adjusted analyses would require larger samples.

Table 3. Sensitivity analyses of the correlations between SUV parameters and fibrosis.

Analysis	*n*	SUVpeak	SUVmean	SUVmax
Primary analysis				
Spearman ρ (*p*)	21	−0.66 (0.001)	−0.54 (0.011)	−0.65 (0.001)
Pearson r (*p*)	21	−0.44 (0.047)	−0.46 (0.038)	−0.47 (0.032)
Repeated fibrosis measurement				
Spearman ρ (*p*)	21	−0.62 (0.003)	−0.52 (0.016)	−0.61 (0.003)
Pearson r (*p*)	21	−0.43 (0.049)	−0.46 (0.035)	−0.47 (0.032)
Excluding influential observation *				
Spearman ρ (*p*)	20	−0.69 (0.001)	−0.57 (0.009)	−0.68 (0.001)
Pearson r (*p*)	20	−0.70 (0.001)	−0.63 (0.003)	−0.66 (0.001)
50% threshold segmentation only				
Spearman ρ (*p*)	14	−0.60 (0.023)	−0.53 (0.054)	−0.53 (0.054)
Pearson r (*p*)	14	−0.27 (0.347)	−0.30 (0.292)	−0.29 (0.320)

SUV, standardized uptake value; SUVpeak, peak SUV (1 cm^3 sphere); SUVmean, mean SUV; SUVmax, maximum SUV. * One patient with SUVmax 20.3 and fibrosis 25.8% (Cook's distance 7.1).

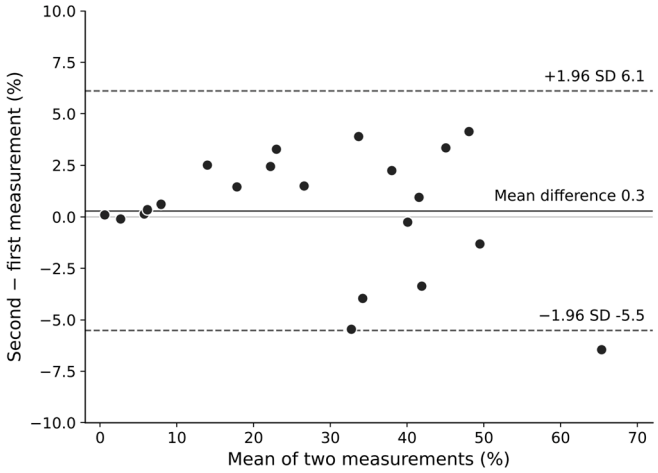


Figure 3. Bland–Altman plot of intraobserver agreement for fibrosis quantification on Masson trichrome-stained sections. The solid line indicates the mean difference between the two measurements, and the dashed lines indicate the 95% limits of agreement (mean difference ± 1.96 standard deviations).

4. Discussion

In this exploratory study of resected PDAC, FDG uptake was inversely associated with stromal fibrosis across all absolute SUV parameters and both fibrosis measurements, and the associations persisted after adjustment for tumor volume and scanner type. The rank-based correlations were moderate to strong (ρ = −0.54 to −0.66), whereas the linear correlations were weaker because of a single tumor with very high FDG uptake. Thus, the estimated strength of the association depended on the analytic method and on a single observation, and the true magnitude may be smaller than the rank-based estimates suggest. Even so, SUV parameters accounted for less than half of the variability in fibrosis, and the 95% CIs were wide. These findings suggest that tumors with more fibrosis tend to show lower FDG uptake, but that FDG PET/CT alone cannot reliably estimate the stromal burden of an individual tumor.

An inverse relationship between fibrosis and FDG uptake is biologically plausible. Dense desmoplastic stroma is characterized by hypovascularity, high interstitial pressure, and a reduced density of tumor cells per unit volume, all of which can limit FDG delivery and accumulation [3,5,25,26]. Stromal stiffening and paracrine signaling from CAFs also modulate tumor cell behavior and metabolism [15,27,28]. However, the collagen proportionate area measured in this study reflects the amount of extracellular matrix rather than the activity of CAFs, and our data cannot establish that collagen itself suppresses glucose metabolism. Differences in tumor cellularity, perfusion, inflammatory infiltrates, and the metabolic activity of tumor cells remain alternative explanations, and the incomplete strength of the association indicates that these factors contribute substantially to FDG uptake independently of fibrosis [6,8]. Of these factors, histological grade was available but could not be analyzed meaningfully because only one tumor was poorly differentiated; tumor cellularity, inflammatory infiltration, and vascularity were not quantified; and individual blood glucose levels were not recorded, although all patients met the institutional criterion of a glucose level below 150 mg/dL. Tumor size may also be relevant, because adjustment for pathological tumor size attenuated the linear correlations. Notably, preclinical studies have shown that the stroma can also restrain tumor progression [29,30], underscoring the need to characterize stromal composition rather than simply its quantity.

The three absolute SUV parameters were almost perfectly intercorrelated and showed associations of similar strength, with no statistically significant differences among them. Thus, in contrast to the emphasis sometimes placed on SUVpeak as a more robust measure [16], our data provide no evidence that any single SUV parameter is superior for reflecting fibrosis; SUVpeak showed the numerically largest rank correlation, but SUVmax performed similarly and may be sufficient in this context. Because the three parameters were nearly collinear ($r \geq 0.984$), they convey largely redundant information, and their associations with fibrosis should not be regarded as independent findings; as each parameter was analyzed separately rather than in a joint model, multicollinearity did not affect the individual estimates. We nevertheless reported all three because SUVmax is the most widely used parameter in clinical practice, SUVpeak is the standardized parameter recommended by PERCIST and is less sensitive to image noise than SUVmax [16], and SUVmean reflects uptake across the segmented tumor volume; their similar results indicate that the findings do not depend on the choice of parameter. The SUVmax/SUVmean and SUVmax/SUVpeak ratios, which we hypothesized might reflect fibrosis-related metabolic heterogeneity, showed no significant association with fibrosis. Moreover, the SUVmax/SUVmean ratio was largely determined by the segmentation method, with nonoverlapping ranges for threshold-based (1.48–1.68) and gradient-based (1.16–1.46) contours, indicating that this ratio cannot be interpreted as a biological measure of heterogeneity when segmentation methods differ. These ratios combine highly correlated measurements and may be too coarse to capture the spatial relationship between stroma and metabolically active tumor cells; dedicated texture or radiomic analyses would be required to test this hypothesis [10,11]. Furthermore, a nonsignificant result in a small sample does not establish the absence of an association.

Several methodological observations may be useful for future studies. First, the fixed 50% threshold failed to delineate one-third of the tumors because of low tumor-to-background contrast, which is common in PDAC, and a gradient-based method was required. Threshold failure occurred mostly in tumors with low FDG uptake (median SUVmax, 3.6 vs. 6.3) that tended to have more fibrosis (median, 40.2% vs. 21.1%); therefore, the choice of segmentation method is not independent of the variables of interest and can affect SUVmean and volume-based parameters, whereas SUVmax and SUVpeak are less dependent on segmentation. We combined the two approaches because forcing a fixed threshold onto lesions in which it extended into adjacent physiological uptake would have

produced volumes that did not represent the tumor, whereas excluding these lesions would have selectively removed low-uptake, highly fibrotic tumors and biased the cohort. The resulting methodological heterogeneity mainly affects SUVmean and MTV, whereas SUVmax and SUVpeak, which are determined by the hottest voxels, are largely independent of the contour. Nevertheless, the Spearman coefficients in tumors segmented with the threshold alone were of similar magnitude to those in the entire cohort, suggesting that the association was not driven by the segmentation method. In this subset, the Pearson coefficients were small and nonsignificant, whereas the Spearman coefficients remained moderate. This divergence is best explained by the small sample size, the skewed SUV distribution, the restricted range of SUV values after the exclusion of low-uptake tumors (SUVmax $\geq$ 4.45), and the leverage of the single high-uptake tumor, because the Pearson coefficients increased markedly after its exclusion, rather than by segmentation-related bias. Nevertheless, estimates from a subgroup of 14 patients are imprecise and should be interpreted with caution. Second, a single patient with very high FDG uptake strongly attenuated the Pearson correlations, illustrating the instability of linear correlation estimates in small samples with skewed SUV distributions and supporting the use of rank-based methods. Third, the image-based quantification of fibrosis showed excellent reproducibility, indicating that measurement error in fibrosis is unlikely to have substantially biased the associations.

Our findings have implications for noninvasive assessment of the tumor microenvironment. Because FDG uptake primarily reflects tumor cell glucose metabolism, its relationship with stromal content is likely to be indirect. Fibroblast activation protein inhibitor (FAPI)-based tracers, which directly target activated CAFs, show high uptake in PDAC and may provide a more direct and specific approach to imaging stromal biology [31]. Integrating nuclear medicine techniques with complementary imaging modalities [32], for example, combining FAPI PET with FDG PET/CT and other imaging and clinical variables, may allow a more comprehensive characterization of the stroma than any single FDG parameter. It should be emphasized that the present study demonstrates only a statistical association at the group level; associations with pathological aggressiveness, treatment response, recurrence, or survival, as well as the ability of SUV parameters to predict fibrosis in individual patients, were not evaluated. Potential clinical applications, such as noninvasive stratification of stromal burden before stroma-targeted therapy, therefore remain hypothetical.

This study has several limitations. First, the sample size was small and was determined by the number of available cases rather than by a formal power calculation, and the study was retrospective and conducted at a single center. These features limit statistical power, the precision and stability of the correlation estimates, and generalizability; although the primary analyses were adjusted for multiple testing, the additional exploratory and subgroup analyses carry a risk of false-positive findings. Second, fibrosis was quantified from selected sections of the resected specimens, which may not represent the spatial heterogeneity of the entire tumor, whereas PET parameters were derived from the whole lesion; this mismatch may have attenuated the associations. Sampling one to three representative sections and 5–10 fields per patient cannot fully capture the marked regional heterogeneity of PDAC stroma, and whole-slide or multiregional sampling co-registered with PET would be preferable in future studies. Third, two PET/CT scanners were used over the study period, and SUV measurements are affected by scanner type, reconstruction protocol, partial-volume effects in small lesions, and blood glucose levels [18,33,34]. Although adjustment for scanner type and tumor volume did not change the results, individual glucose values were not available for correction. In addition, two tumors initially considered to be PDAC were reclassified as non-ductal neoplasms on pathological re-review; because PDAC and other pancreatic neoplasms can show overlapping features on preoperative imaging [35], histolog-

ical confirmation is essential for studies of PDAC-specific imaging–pathology correlations. Fourth, fibrosis was quantified by a single observer; only intraobserver reproducibility of the collagen proportionate area was assessed, and interobserver agreement was not tested. Interobserver reproducibility should be determined in future studies. Fifth, clinical outcomes, diagnostic thresholds, and the predictive performance of SUV parameters were not evaluated. Accordingly, our findings should be regarded as hypothesis-generating and require external validation.

5. Conclusions

In this exploratory study of 21 patients with resected PDAC, FDG PET/CT-derived SUV parameters showed an inverse association with stromal fibrosis that was moderate in rank-based analyses but weaker in linear analyses and influenced by a single high-uptake tumor. No single SUV parameter performed better than the others, and simple SUV ratios were not associated with fibrosis. These preliminary findings suggest that FDG PET/CT may provide indirect information on tumor stromal characteristics, but they do not support its use as a surrogate for histological assessment of fibrosis. Validation in larger, preferably prospective and multicenter, cohorts is required before any clinical application can be considered, and stroma-targeted imaging may help clarify the relationship between the tumor stroma and PET findings in PDAC.

Author Contributions: Conceptualization, T.J.J. and S.J.L.; Methodology, T.J.J. and B.J.L.; Validation, T.J.J. and B.J.L.; Formal Analysis, T.J.J. and B.J.L.; Investigation, T.J.J.; Data Curation, T.J.J., S.J.L. and B.J.L.; Writing—Original Draft Preparation, T.J.J.; Writing—Review and Editing, T.J.J., S.J.L. and B.J.L.; Project Administration, T.J.J.; Funding Acquisition, T.J.J. and S.J.L. All authors have read and agreed to the published version of the manuscript.

Funding: This research was funded by the Research Fund for faculty of Yonsei University College of Medicine, grant number 6-2015-0033.

Institutional Review Board Statement: The study was conducted in accordance with the Declaration of Helsinki and approved by the Institutional Review Board of Gangnam Severance Hospital (protocol code 3-2015-0436).

Informed Consent Statement: Patient consent was waived due to the retrospective design of the study and the use of anonymized data obtained during routine clinical care. No identifiable patient information is included in this manuscript.

Data Availability Statement: The raw data supporting the conclusions of this article are available from the corresponding author on reasonable request.

Acknowledgments: During the preparation of this study, the authors used Claude (Anthropic; model claude-opus-5-5) for the purposes of writing statistical analysis code, preparing figures, and drafting and editing the manuscript text. The authors have reviewed and edited the output and take full responsibility for the content of this publication.

Conflicts of Interest: The authors declare no conflicts of interest. The funder had no role in the design of the study; in the collection, analyses, or interpretation of data; in the writing of the manuscript; or in the decision to publish the results.

Abbreviations

The following abbreviations are used in this manuscript:

AJCC	American Joint Committee on Cancer
CAF	cancer-associated fibroblast
CI	confidence interval
FAPI	fibroblast activation protein inhibitor

FDG	^{18}F-fluorodeoxyglucose
ICC	intraclass correlation coefficient
IQR	interquartile range
MTV	metabolic tumor volume
OSEM	ordered-subset expectation maximization
PDAC	pancreatic ductal adenocarcinoma
PET/CT	positron emission tomography/computed tomography
SUV	standardized uptake value
SUVmax	maximum standardized uptake value
SUVmean	mean standardized uptake value
SUVpeak	peak standardized uptake value

References

1. Siegel, R.L.; Kratzer, T.B.; Giaquinto, A.N.; Sung, H.; Jemal, A. Cancer statistics, 2025. *CA Cancer J. Clin.* **2025**, *75*, 10–45. [CrossRef] [PubMed]
2. Kleeff, J.; Korc, M.; Apte, M.; La Vecchia, C.; Johnson, C.D.; Biankin, A.V.; Neale, R.E.; Tempero, M.; Tuveson, D.A.; Hruban, R.H.; et al. Pancreatic cancer. *Nat. Rev. Dis. Primers* **2016**, *2*, 16022. [PubMed]
3. Erkan, M.; Hausmann, S.; Michalski, C.W.; Fingerle, A.A.; Dobritz, M.; Kleeff, J.; Friess, H. The role of stroma in pancreatic cancer: Diagnostic and therapeutic implications. *Nat. Rev. Gastroenterol. Hepatol.* **2012**, *9*, 454–467. [CrossRef] [PubMed]
4. Provenzano, P.P.; Cuevas, C.; Chang, A.E.; Goel, V.K.; Von Hoff, D.D.; Hingorani, S.R. Enzymatic targeting of the stroma ablates physical barriers to treatment of pancreatic ductal adenocarcinoma. *Cancer Cell* **2012**, *21*, 418–429. [CrossRef] [PubMed]
5. Olive, K.P.; Jacobetz, M.A.; Davidson, C.J.; Gopinathan, A.; McIntyre, D.; Honess, D.; Madhu, B.; Goldgraben, M.A.; Caldwell, M.E.; Allard, D.; et al. Inhibition of Hedgehog signaling enhances delivery of chemotherapy in a mouse model of pancreatic cancer. *Science* **2009**, *324*, 1457–1461. [CrossRef] [PubMed]
6. Wang, L.M.; Silva, M.A.; D'Costa, Z.; Bockelmann, R.; Soonawalla, Z.; Liu, S.; O'Neill, E.; Mukherjee, S.; McKenna, W.G.; Muschel, R.; et al. The prognostic role of desmoplastic stroma in pancreatic ductal adenocarcinoma. *Oncotarget* **2016**, *7*, 4183–4194. [CrossRef] [PubMed]
7. Neesse, A.; Michl, P.; Frese, K.K.; Feig, C.; Cook, N.; Jacobetz, M.A.; Lolkema, M.P.; Buchholz, M.; Olive, K.P.; Gress, T.M.; et al. Stromal biology and therapy in pancreatic cancer. *Gut* **2011**, *60*, 861–868. [CrossRef] [PubMed]
8. Sherman, M.H.; Beatty, G.L. Tumor microenvironment in pancreatic cancer pathogenesis and therapeutic resistance. *Annu. Rev. Pathol. Mech. Dis.* **2023**, *18*, 123–148. [CrossRef] [PubMed]
9. Lee, J.W.; Kang, C.M.; Choi, H.J.; Lee, W.J.; Song, S.Y.; Lee, J.H.; Lee, J.D. Prognostic value of metabolic tumor volume and total lesion glycolysis on preoperative ^{18}F-FDG PET/CT in patients with pancreatic cancer. *J. Nucl. Med.* **2014**, *55*, 898–904. [CrossRef] [PubMed]
10. Hyun, S.H.; Kim, H.S.; Choi, S.H.; Choi, D.W.; Lee, J.K.; Lee, K.H.; Park, J.O.; Lee, K.-H.; Kim, B.-T.; Choi, J.Y. Intratumoral heterogeneity of ^{18}F-FDG uptake predicts survival in patients with pancreatic ductal adenocarcinoma. *Eur. J. Nucl. Med. Mol. Imaging* **2016**, *43*, 1461–1468. [CrossRef] [PubMed]
11. Yoo, S.H.; Kang, S.Y.; Cheon, G.J.; Oh, D.Y.; Bang, Y.J. Predictive role of temporal changes in intratumoral metabolic heterogeneity during palliative chemotherapy in patients with advanced pancreatic cancer: A prospective cohort study. *J. Nucl. Med.* **2020**, *61*, 33–39. [CrossRef] [PubMed]
12. Ahn, S.J.; Park, M.-S.; Lee, J.D.; Kang, W.J. Correlation between ^{18}F-fluorodeoxyglucose positron emission tomography and pathologic differentiation in pancreatic cancer. *Ann. Nucl. Med.* **2014**, *28*, 430–435. [CrossRef] [PubMed]
13. Choi, H.J.; Kang, C.M.; Lee, W.J.; Song, S.Y.; Cho, A.; Yun, M.; Lee, J.D.; Kim, J.H.; Lee, J.H. Prognostic value of ^{18}F-fluorodeoxyglucose positron emission tomography in patients with resectable pancreatic cancer. *Yonsei Med. J.* **2013**, *54*, 1377–1383. [CrossRef] [PubMed]
14. Okamoto, K.; Koyama, I.; Miyazawa, M.; Toshimitsu, Y.; Aikawa, M.; Okada, K.; Imabayashi, E.; Matsuda, H. Preoperative ^{18}[F]-fluorodeoxyglucose positron emission tomography/computed tomography predicts early recurrence after pancreatic cancer resection. *Int. J. Clin. Oncol.* **2011**, *16*, 39–44. [CrossRef] [PubMed]
15. Meng, Q.; Fang, Z.; Mao, X.; Tang, R.; Liang, C.; Hua, J.; Wang, W.; Shi, S.; Yu, X.; Xu, J. Metabolic reprogramming of cancer-associated fibroblasts in pancreatic cancer contributes to the intratumor heterogeneity of PET-CT. *Comput. Struct. Biotechnol. J.* **2023**, *21*, 2631–2639. [CrossRef] [PubMed]
16. Wahl, R.L.; Jacene, H.; Kasamon, Y.; Lodge, M.A. From RECIST to PERCIST: Evolving considerations for PET response criteria in solid tumors. *J. Nucl. Med.* **2009**, *50*, 122S–150S. [CrossRef] [PubMed]
17. Amin, M.B.; Edge, S.B.; Greene, F.L.; Byrd, D.R.; Brookland, R.K.; Washington, M.K.; Gershenwald, J.E.; Compton, C.C.; Hess, K.R.; Sullivan, D.C.; et al. (Eds.) *AJCC Cancer Staging Manual*, 8th ed.; Springer: New York, NY, USA, 2017.

18. Boellaard, R.; Delgado-Bolton, R.; Oyen, W.J.G.; Giammarile, F.; Tatsch, K.; Eschner, W.; Verzijlbergen, F.J.; Barrington, S.F.; Pike, L.C.; Weber, W.A.; et al. FDG PET/CT: EANM procedure guidelines for tumour imaging: Version 2.0. *Eur. J. Nucl. Med. Mol. Imaging* **2015**, *42*, 328–354. [CrossRef] [PubMed]
19. Werner-Wasik, M.; Nelson, A.D.; Choi, W.; Arai, Y.; Faulhaber, P.F.; Kang, P.; Almeida, F.D.; Xiao, Y.; Ohri, N.; Brockway, K.D.; et al. What is the best way to contour lung tumors on PET scans? Multiobserver validation of a gradient-based method using a NSCLC digital PET phantom. *Int. J. Radiat. Oncol. Biol. Phys.* **2012**, *82*, 1164–1171. [CrossRef] [PubMed]
20. Schneider, C.A.; Rasband, W.S.; Eliceiri, K.W. NIH Image to ImageJ: 25 years of image analysis. *Nat. Methods* **2012**, *9*, 671–675. [CrossRef] [PubMed]
21. Schober, P.; Boer, C.; Schwarte, L.A. Correlation coefficients: Appropriate use and interpretation. *Anesth. Analg.* **2018**, *126*, 1763–1768. [CrossRef] [PubMed]
22. Steiger, J.H. Tests for comparing elements of a correlation matrix. *Psychol. Bull.* **1980**, *87*, 245–251. [CrossRef]
23. Koo, T.K.; Li, M.Y. A guideline of selecting and reporting intraclass correlation coefficients for reliability research. *J. Chiropr. Med.* **2016**, *15*, 155–163. [CrossRef] [PubMed]
24. Bland, J.M.; Altman, D.G. Statistical methods for assessing agreement between two methods of clinical measurement. *Lancet* **1986**, *1*, 307–310. [CrossRef]
25. Apte, M.V.; Wilson, J.S.; Lugea, A.; Pandol, S.J. A starring role for stellate cells in the pancreatic cancer microenvironment. *Gastroenterology* **2013**, *144*, 1210–1219. [CrossRef] [PubMed]
26. Koay, E.J.; Truty, M.J.; Cristini, V.; Thomas, R.M.; Chen, R.; Chatterjee, D.; Kang, Y.; Bhosale, P.; Tamm, E.P.; Crane, C.H.; et al. Transport properties of pancreatic cancer describe gemcitabine delivery and response. *J. Clin. Investig.* **2014**, *124*, 1525–1536. [CrossRef] [PubMed]
27. Rath, N.; Olson, M.F. Regulation of pancreatic cancer aggressiveness by stromal stiffening. *Nat. Med.* **2016**, *22*, 462–463. [CrossRef] [PubMed]
28. Bazzichetto, C.; Conciatori, F.; Falcone, I.; Cognetti, F.; Milella, M.; Ciuffreda, L. Advances in tumor-stroma interactions: Emerging role of cytokine network in colorectal and pancreatic cancer. *J. Oncol.* **2019**, *2019*, 5373580. [CrossRef] [PubMed]
29. Özdemir, B.C.; Pentcheva-Hoang, T.; Carstens, J.L.; Zheng, X.; Wu, C.C.; Simpson, T.R.; Laklai, H.; Sugimoto, H.; Kahlert, C.; Novitskiy, S.V.; et al. Depletion of carcinoma-associated fibroblasts and fibrosis induces immunosuppression and accelerates pancreas cancer with reduced survival. *Cancer Cell* **2014**, *25*, 719–734. [CrossRef] [PubMed]
30. Rhim, A.D.; Oberstein, P.E.; Thomas, D.H.; Mirek, E.T.; Palermo, C.F.; Sastra, S.A.; Dekleva, E.N.; Saunders, T.; Becerra, C.P.; Tattersall, I.W.; et al. Stromal elements act to restrain, rather than support, pancreatic ductal adenocarcinoma. *Cancer Cell* **2014**, *25*, 735–747. [CrossRef] [PubMed]
31. Kratochwil, C.; Flechsig, P.; Lindner, T.; Abderrahim, L.; Altmann, A.; Mier, W.; Adeberg, S.; Rathke, H.; Rohrich, M.; Winter, H.; et al. ^{68}Ga-FAPI PET/CT: Tracer uptake in 28 different kinds of cancer. *J. Nucl. Med.* **2019**, *60*, 801–805. [CrossRef] [PubMed]
32. Archibald, S.J.; Holland, J.P.; Korde, A.; Martins, A.F.; Shuhendler, A.J.; Scott, P.J.H. Combining nuclear medicine with other modalities: Future prospect for multimodality imaging. *Mol. Imaging* **2024**, *23*, 15353508241245265. [CrossRef] [PubMed]
33. Soret, M.; Bacharach, S.L.; Buvat, I. Partial-volume effect in PET tumor imaging. *J. Nucl. Med.* **2007**, *48*, 932–945. [CrossRef] [PubMed]
34. Lee, S.M.; Kim, T.-S.; Lee, J.W.; Kim, S.-K.; Park, S.-J.; Kim, J.H.; Kim, Y.H.; Kim, J.S.; Kim, J.Y.; Kim, J.H. Improved prognostic value of standardized uptake value corrected for blood glucose level in pancreatic cancer using F-18 FDG PET. *Clin. Nucl. Med.* **2011**, *36*, 331–336. [CrossRef] [PubMed]
35. Yu, J.; Cao, Y.; Xia, F.; Lan, Q.; Zhou, J.; Wang, Z.; Ren, S. Diagnostic performance of multislice spiral computed tomography in differentiating pancreatic acinar cell carcinoma from pancreatic ductal adenocarcinoma. *Abdom. Radiol.* **2026**, *51*, 6664–6672. [CrossRef] [PubMed]

Disclaimer/Publisher's Note: The statements, opinions and data contained in all publications are solely those of the individual author(s) and contributor(s) and not of MDPI and/or the editor(s). MDPI and/or the editor(s) disclaim responsibility for any injury to people or property resulting from any ideas, methods, instructions or products referred to in the content.